Model of a Hollow Cathode Insert Plasma

I.G. Mikellides*, I. Katz†, D.M. Goebel‡ and J.E. Polk§
Jet Propulsion Laboratory, California Institute of Technology, Pasadena, CA, 91109

A 2-D axisymmetric fluid model of the plasma in the insert region of a hollow cathode is presented. The level of sophistication included in the model is motivated in part by the need to determine quantitatively plasma fluxes to the emitter surface. The ultimate goal is to assess whether plasma effects can degrade the life of impregnated inserts beyond those documented throughout the 30-50 year history of vacuum cathode technologies. Results from simulations of a 1.2-cm diameter cathode operating at a discharge current of 25 A, and a gas flow rate of 5 sccm, suggest that approximately 10 A of electron current, and 3.5 A of ion current return to the emitter surface. The total emitted electron current computed by the model is about 35 A. Comparisons with plasma measurements suggest that anomalous heating of the plasma due to two-stream instabilities is possible near the orifice region. Solution to the heavy species energy equation, with classical transport and no viscous effects, predicts heavy species temperatures as high as 2640 °K.

Nomenclature

Main Variables

A	=	area (m^2)
$\bar{c}$	=	mean particle speed (m/s)
e	=	electron charge (C)
E	=	Electric field (V/m)
f	=	coefficient of friction ($kg/m^3/s$)
j	=	current density (A/m^2)
Kn	=	Knudsen number (λ/channel diameter)
k	=	Boltzmann constant (1.3806e-23 J/°K)
L	=	length
M	=	molecular weight (amu)
m	=	particle mass (kg)
n	=	particle density (m^{-3})
$\hat{\mathbf{n}}$	=	unit vector normal to surface
$\dot{n}$	=	ionization rate ($s^{-1}m^{-3}$)
p	=	pressure (Pa)
Q	=	heat exchange by elastic collisions ($kg/m/s^3$)
q	=	conductive heat flux (W/m^2)
R	=	collisional (friction) force density ($kg/m^2/s^2$)
S	=	energy loss by inelastic collisions ($kg/m/s^3$)
T	=	temperature (°K)
T	=	temperature (eV)
$\overline{T}$	=	characteristic temperature for Xe

Subscripts, continued

i	=	ion
ins	=	insert
iz	=	ionization
n	=	neutral
orf	=	orifice
s	=	species type
w	=	wall
WF	=	work function
SH	=	Schottky

Superscripts

em	emitted
ab	absorbed

Greek symbols

α	=	Richardson constant (=1.2017e6 $A/m^2/°K^2$)
Γ	=	general flux vector
ΔT	=	total insert temperature variation (°K)
δ	=	xenon atom diameter (Å)
ε	=	ionization potential (eV)
ε_0	=	permittivity (free space, =8.8542e-12 F/m)
η	=	classical plasma resistivity (m Ohm)

* Senior Scientist, Advanced Propulsion Technology Group, 4800 Oak Grove Drive, Pasadena, CA, 91109, Mail Stop 125-109, Member AIAA.
† Group Supervisor, Advanced Propulsion Technology Group, 4800 Oak Grove Drive, Pasadena, CA, 91109, Mail Stop 125-109, Senior Member AIAA.
‡ Principal Scientist, Advanced Propulsion Technology Group, 4800 Oak Grove Drive, Pasadena, CA, 91109, Mail Stop 125-109, Member AIAA.
§ Principal Scientist, Advanced Propulsion Technology Group, 4800 Oak Grove Drive, Pasadena, CA, 91109, Mail Stop 125-109, Senior Member AIAA.

t	=	time (s)	κ	=	thermal conductivity (W/m/°K)
u	=	velocity (m/s)	λ	=	mean free path (m)
V	=	volume (m^3)	ν	=	collision frequency (s^{-1})
			σ	=	collision cross sectional area (m^2)
Subscripts			ϕ	=	plasma potential (V)
a	=	species type	Ω	=	collision integral parameter for Xe
B	=	Bohm	ω	=	plasma frequency (s^{-1})
e	=	electron	σ	=	collision cross sectional area (m^2)
eff	=	effective	ϕ	=	plasma potential (V)

I. Introduction

HOLLOW cathodes have been studied extensively since the early 1930's due to their wide range of applicability in vacuum microelectronic devices, microwave tubes, pseudosparks, lasers and materials processing. Over the past decade, hollow cathodes have also become critical components in many electric propulsion systems such as ion propulsion and Hall-effect thrusters. The longest operations of hollow cathodes for space applications were achieved during the International Space Station (ISS) plasma contactor test at the NASA Glenn Research Center (GRC)[1] and during the Extended Life Test of the NASA Solar Electric Propulsion Technology Applications Readiness (NSTAR) engine at the Jet Propulsion Laboratory (JPL).[2] After 28,000 hrs of operation the ISS contactor failed to restart; upon conclusion of the NSTAR ELT the main discharge chamber and neutralizer cathodes had been operating without problems after 30,252 hrs. The lifetime requirements of these devises for long duration missions proposed under NASA's Project Prometheus, such as the Jupiter Icy Moons Orbiter (JIMO), may exceed 80,000 hrs. For JIMO, it would not be feasible to conclude life tests of this duration and flight qualify the system before the proposed earliest launch date (2015). To address this need an intense effort has been underway at JPL that combines theoretical modeling and experiment to quantify the plasma environment in these devices. The ultimate goal is to identify the mechanisms that cause performance degradation and failure at the required operating levels.

Cathodes made of porous tungsten inserts that are impregnated with barium aluminates are potential candidates to meet the performance and lifetime requirements for JIMO and other long missions proposed by NASA. Empirical studies on impregnated cathodes in diodes and traveling-wave tubes, carried out in the late 1970's by Palluel and Schroff,[3] showed that lifetime is largely determined by the rate at which the emitting material is depleted. Barium depletion rates in that study were found to follow a $t^{1/2}$ law. More importantly, the measured depletion depths showed a marked dependence on the cathode operating temperature. For example, after 2500 hrs the barium depleted depth in an S-type cathode was found to be about a factor of 3 higher when the cathode temperature was 1230 °C compared to 1035°C. The trend was observed in the depletion depth measurements for a variety of operating conditions and cathode types that were impregnated with barium/calcium aluminates. Lifetimes recorded for various commercial microwave tubes provide further evidence of the dependence of cathode lifetime on operating temperature. For example, in a TWT (radio link) tube for which the rated cathode temperature was 1050 °C, the recorded lifetime was 70,000 hrs. By comparison, an O-type carcinotron lasted only 2000 hrs; its rated cathode temperature was 1250 °C.

To apply the wealth of information acquired for vacuum tube cathode technologies to cathodes intended for use in high power propulsion systems one main question must be answered: what is the effect of the plasma on the emission characteristics? Although the lifetime of the microwave tube cathodes mentioned above showed a marked dependence on operating temperature, they were also rated for current densities much lower than those required for high power propulsion applications such as JIMO. To answer this question, the plasma environment in the insert region must be quantified. Specifically, particle and heat fluxes to the insert walls must be determined in order to assess their effect on the insert temperature and evaporation rates of the barium constituents.

Access to the hollow cathode insert plasma by empirical techniques is difficult and has been mostly limited to measurements along the axis of symmetry. Siegfried and Wilbur[4] measured plasma properties in the insert region of a 6.4-mm (outer) diameter hollow cathode, operating with mercury, up to discharge currents of 9 A. Salhi and Turchi[5] also measured plasma properties in 6.4-mm cathode at several amperes and a few sccm, operating with xenon. A number of other experimental investigations on low-current cathodes for space applications have also taken place since the 1960's at NASA GRC, Hughes Research Laboratories and other institutions.[6,7,8,9] A few efforts to model the plasma in the insert region have also been reported. Siegfried[10] developed a phenomenological (0-D) model of the mercury cathode to predict to first order cathode operating parameters such as emission length and insert temperature. The analytical formulation was based on an idealized "ion production region." Salhi and Turchi[11] also developed a first principles model which included 2-D variation of the plasma properties, in which the gas

temperature was set equal to the wall temperature, and a two temperature, (equilibrium) Saha equation was used to compute the neutral particle density. Ohmic heating of the plasma was determined using the electrical conductivity for fully-ionized plasma (Spitzer).

Over the past year a systematic investigation of cathodes for high power electric propulsion (>25 kW per engine), has been underway at JPL. The goal of the effort is to rigorously quantify the effects of the plasma in cathodes with requirements set by long duration missions (>80,000 hrs). Recent measurements in a laboratory model hollow cathode at JPL, operating at 25 A and various gas flow rates, has shown noticeably different plasma properties in the insert region compared to previous investigations. The most noticeable distinction compared to the Siegfried[4] and the Salhi[5] data has been the non-monotonic variation of the electron density measured along the insert axis of symmetry.[12] A recent effort by Katz, et al.[13] to model the insert plasma under these operating conditions included the effects of ion-neutral and electron-neutral collisions on plasma diffusion, but the results supported the previous observations of a monotonically decreasing density upstream of the orifice.

We describe in this paper a new 2-D axisymmetric model of the hollow cathode insert region. The multi-component fluid in this region is assumed to consist of ions, electrons and neutral atoms. We present results from the model, and validate it with recent experimental measurements obtained in a laboratory hollow cathode under high-current operating conditions. The model may be used to quantify all pertinent variables along the insert wall (e.g. particle and heat fluxes), and later may be combined with particle tracing to predict the migration of barium particles in the insert region.

II. Theoretical Model

A. Background

The hollow cathode insert region consists mainly of a metal tube lined with a sintered tungsten insert. The insert is impregnated with a low work function medium, usually barium and calcium oxide aluminates, to allow electron emission when heated to temperatures above ~1000 °C. The cathode channel is capped at one end by a plate with a small orifice at its center. The operating gas, usually xenon in cathodes intended for use in ion propulsion, is fed into the tube at the opposite end of the channel as shown in Figure 1. Electrons emitted from the insert are attracted by a positively-biased (enclosed) keeper electrode downstream of the orifice. The emitted electrons also have sufficient energy to ionize part of the neutral gas. The evolution of ionized particles in the insert region depends on a variety of physical processes that are inherently two-dimensional.

The region of the hollow cathode that is modeled in this effort is depicted by the dashed line in Figure 1. The gaseous material in the region consists of a weakly ionized, highly collisional plasma. Although anomalous effects are possible (as it will be shown later), the dominant mechanisms that determine the transport of charge, mass and heat in the plasma are classical collisions that occur between electrons and neutrals (e-n), electrons and ions (e-i) and, ions and neutrals (i-n). The latter is mainly due to resonant charge exchange between fast ions and slow neutrals with an associated average collision cross section in the order of 100 A. Table 1 lists average values of mean free paths associated with insert region plasma. Under the operating conditions of interest, the mean free paths associated with these particle collisions are all small compared to the hollow cathode channel size ($0.002<Kn<0.2$). Our theoretical model is therefore based on a "fluid" approach, which assumes that particles are perturbed from their Maxwellian distribution function only by virtue of collisions, and relax to their equilibrium distribution within the mean time between collisions.

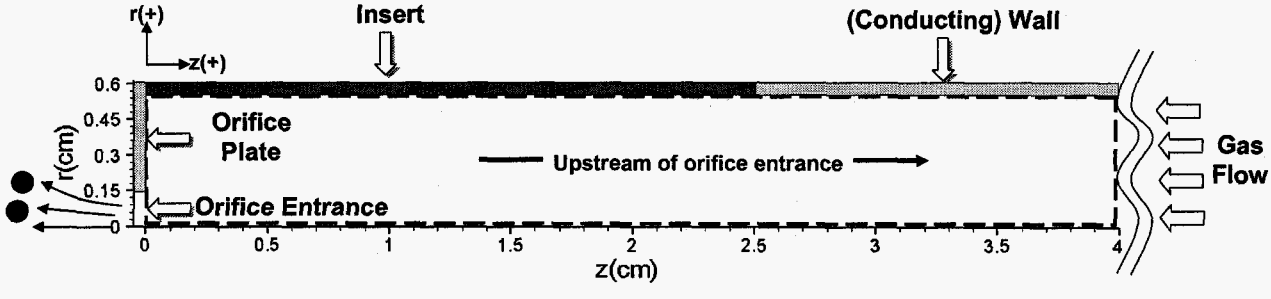

Figure 1. Basic setup used for the insert plasma model.

The equations that describe the behavior of macroscopic parameters, such as n, $\mathbf{u}_s$, T_e etc., can be obtained directly from the kinetic equations, and have been derived by many authors. We base our approach on the formulations first deduced by S.I. Braginskii[14] due to the elucidatory form in which the transport equations have been derived for a general binomial system of colliding particles in the presence of electromagnetic fields.

Table 1. Characteristic lengths and times for the hollow cathode insert plasma under investigation. Nominal operating conditions used in this study: discharge current of 25 A, gas flow rate of 5 sccm, no applied magnetic field.

Orifice Entrance n=5e19m^{-3}, T_e=2eV, n_n=5e21 m^{-3}, T=3000 °K , $\bar{u}_n$=5 m/s	Dense Plasma Region n=2e20m^{-3}, T_e=1.8eV n_n=3e21 m^{-3}, T=3600 °K, $\bar{u}_n$=5 m/s
ν_{en}^{-1}=1.7e-9 s, $\lambda_{en} \approx 1.0$ mm	ν_{en}^{-1}=3.3e-9 s, $\lambda_{en} \approx 1.85$ mm
ν_{ei}^{-1}=2.4e-9 s, $\lambda_{ei} \approx 1.4$ mm	ν_{ei}^{-1}=0.56e-9 s, $\lambda_{ei} \approx 0.32$ mm
ν_{in}^{-1}=2.9e-7 s, $\lambda_{in} \approx 0.2$ mm	ν_{in}^{-1}=4.4e-7 s, $\lambda_{in} \approx 0.33$ mm
ν_{iz}^{-1}=1.7e-6 s, $\lambda_{iz} \approx 0.09$ mm	ν_{iz}^{-1}=6.1e-6 s, $\lambda_{iz} \approx 0.031$ mm
ω_e^{-1}=1.7e-9 s, $\omega_e(\nu_{en}+\nu_{ei})^{-1}$=0.58	ω_e^{-1}=9.0e-8 s, $\omega_e(\nu_{en}+\nu_{ei})^{-1}$=0.005

B. Governing Equations

1. Conservation of mass

Under the assumptions of quasi-neutrality ($n \equiv n_e = n_i$) and single ionization, species continuity for the plasma is expressed by,

$$\frac{\partial n}{\partial t} + \nabla \cdot (n\mathbf{u}_e) = \dot{n} \tag{1}$$

for the electrons and by,

$$\frac{\partial n}{\partial t} + \nabla \cdot (n\mathbf{u}_i) = \dot{n} \tag{2}$$

for the ions. The ionization rate is given by,

$$\dot{n} = n\nu_{iz}, \qquad \nu_{iz} \equiv n_n \langle \sigma_{iz}\mathbf{u}_e \rangle \tag{3}$$

The product $n_n\langle\sigma_{iz}\mathbf{u}_e\rangle$ is termed the "ionization collision frequency", ν_{iz}. The ionization collision cross section is a known function of temperature for xenon $\sigma_{iz} = \sigma_{iz}(T_e)$, and is incorporated in the model as a polynomial fit to measurements obtained by M. Hayashi.[15] We approximate that $\langle\sigma_{iz}\mathbf{u}_e\rangle \approx \sigma_{iz}(T_e)\,\bar{c}_e$.

2. Conservation of momentum

The most general form of the momentum equation for species "s" colliding with species "a" in the absence of a magnetic field (B=0) is expressed by:

$$n_s m_s \frac{D\mathbf{u}_s}{Dt} = n_s q_s \mathbf{E} - \nabla \cdot \mathbf{p}_s + \mathbf{R}_s, \qquad \mathbf{R}_s \equiv \sum_a \mathbf{R}_{sa} = -\sum_a f_{sa}(\mathbf{u}_s - \mathbf{u}_a) \tag{4}$$

where $\mathbf{R}_{sa}$ denotes the mean change in momentum of particles "s" due to collision with particles "a", and D/Dt $\equiv \partial/\partial t + \mathbf{u}_s \cdot \nabla$ is the material derive. Since $\mathbf{R}_{sa}$ is related to the rate of momentum transfer between species by collisions it is many times identified as a "friction" or "drag" term in the momentum equation. However, it should not be confused with fluid viscosity which is a direct consequence of gradients in velocity field, and which we neglect in

this work. Finally, it is noted that in its most general form $\mathbf{R}_{sa}$ also includes a force component that arises by virtue of gradients in the temperature of species "s", the so-called thermoelectric force,[16,14] which we neglect in this work.

We identify the quantity f_{sa} above as the coefficient of friction:

$$f_{sa} = n_s m_{sa} \nu_{sa}, \qquad \nu_{sa} \equiv n_a \langle \sigma u \rangle_{sa} \tag{5}$$

Again, we have defined the quantity ν_{sa} as the rate of momentum transfer by collisions from species "s" to species "a," also commonly referred to as the "collision frequency" (which should not be misinterpreted as the number of collisions per unit time). Momentum conservation during the collision leads to,

$$\mathbf{R}_{sa} = -\mathbf{R}_{as} \tag{6}$$

We assume that all dominant processes in the hollow cathode insert plasma are "slow" enough to neglect the inertia terms in both the ion and electron momentum equations. This is implies that no high frequency phenomena (such us MHD waves), or substantial plasma acceleration (compared to $u_s \nu_{sa}$) take place in the insert region. Thus for electrons and ions we write the respective momentum conservation equations as follows:

$$\begin{aligned} 0 &= -ne\mathbf{E} - \nabla p_e - nm_e\left[\nu_{ei}(\mathbf{u}_e - \mathbf{u}_i) + \nu_{en}(\mathbf{u}_e - \mathbf{u}_n)\right] \\ &\approx -ne\mathbf{E} - \nabla p_e - \mathbf{R}_{ei} - nm_e \nu_{en} \mathbf{u}_e \end{aligned} \tag{7}$$

$$\begin{aligned} 0 &= ne\mathbf{E} - \nabla p_i - nm_i\left[\nu_{ie}(\mathbf{u}_i - \mathbf{u}_e) + \nu_{in}(\mathbf{u}_i - \mathbf{u}_n)\right] \\ &\approx ne\mathbf{E} - \nabla p_i - \mathbf{R}_{ie} - nm_i \nu_{in} \mathbf{u}_i \end{aligned} \tag{8}$$

Where we have assumed that neutrals move very slowly compared to ions $\mathbf{u}_i >> \mathbf{u}_n$, and electrons, $\mathbf{u}_e >> \mathbf{u}_n$. We have also reduced the pressure tensor to its scalar, $\mathbf{p}=p\mathbf{I}$ ($\mathbf{I}$=unit matrix).

3. Conservation of energy

The equation for the transport of internal energy of the flow of species "s" in the presence of species "a", in the absence of viscous effects, may be written as,

$$\frac{\partial}{\partial t}\left(n_s m_s \frac{u_s^2}{2} + \frac{3}{2} p_s\right) + \nabla \cdot \left[\left(n_s m_s \frac{u_s^2}{2} + \frac{5}{2} p_s\right)\mathbf{u}_s + \mathbf{q}_s\right] = q_s n_s \mathbf{E} \cdot \mathbf{u}_s + \mathbf{R}_s \cdot \mathbf{u}_s + Q_s - S_s \tag{9}$$

In the absence of the inelastic energy loss term S_s, equation (9) is in a form derived in Ref. 14. The first two RHS terms express the rate of work done by the electric field, $\mathbf{E}\mathbf{j}_s$, and the "friction" forces, $\mathbf{R}_s\mathbf{u}_s$, respectively. The generation of thermal heating Q_s arises by virtue of the different species temperatures.

Conservation of energy during an elastic collision yields the relationship between the thermal and frictional forces:

$$Q_{sa} + Q_{as} + \mathbf{R}_{sa} \cdot \mathbf{u}_s + \mathbf{R}_{as} \cdot \mathbf{u}_a = Q_{sa} + Q_{as} + \mathbf{R}_{sa} \cdot (\mathbf{u}_s - \mathbf{u}_a) = 0 \tag{10}$$

In the present problem it is convenient to eliminate the kinetic energy terms msus2/2 using the species momentum and continuity equations, to obtain an equation for the transport of internal energy:

$$\frac{\partial}{\partial t}\left(\frac{3}{2} p_s\right) + \nabla \cdot \left[\frac{5}{2} p_s \mathbf{u}_s + \mathbf{q}_s\right] - \mathbf{u}_s \cdot \nabla p_s = Q_s - S_s \tag{11}$$

For electrons, using $\mathbf{j}_e$=-en$\mathbf{u}_e$ we write

$$\frac{\partial}{\partial t}\left(\frac{3}{2} n e T_e\right) - \nabla \cdot \left(\frac{5}{2} T_e \mathbf{j}_e + \kappa_e \nabla T_e\right) + \mathbf{j}_e \cdot \frac{\nabla(n T_e)}{n} = Q_e - S_e \tag{12}$$

In equation (12) above, the classical electron thermal conductivity for singly ionized plasma (in W/m/eV), parallel to the magnetic field is given in the appendix.

For Maxwellian distributions functions and for $T=T_n=T_i$ the energy exchange per unit time between electrons and heavy species is given by,[14]

$$Q_{ie} \approx \nu_{ei} n \frac{2m_e}{m} \frac{3}{2} k(T_e - T) \qquad Q_{ne} \approx \nu_{en} n \frac{2m_e}{m} \frac{3}{2} k(T_e - T) \tag{13}$$

Thus, using equation (10) we obtain the electron heating term from elastic collisions as follows:

$$\begin{aligned} Q_e &= Q_{ei} + Q_{en} = -Q_{ne} - Q_{ie} - \mathbf{R}_{ei} \cdot (\mathbf{u}_e - \mathbf{u}_i) - \mathbf{R}_{en} \cdot (\mathbf{u}_e - \mathbf{u}_n) \\ &\approx -(\nu_{ei} + \nu_{en}) n \frac{2m_e}{m} \frac{3}{2} k(T_e - T) - \mathbf{R}_{ei} \cdot (\mathbf{u}_e - \mathbf{u}_i) - \mathbf{R}_{en} \cdot (\mathbf{u}_e - \mathbf{u}_n) \end{aligned} \tag{14}$$

In general, the electron energy loss term S_e includes contributions from the ionization and excitation of the heavy species. However, for the plasma conditions in the insert region it has been determined that the optical depth for a Doppler-broadened line[17] is more the three orders of magnitude greater than unity. Thus, the plasma is optically thick and the majority of the radiation remains trapped.[18] We also note that electron losses due to ionization are enhanced if the electron kinetic energy $m_e u_e^2/2$ becomes comparable to ε_i. Under the conditions of interest however, $\varepsilon >> m_e u_e^2/2$, and so we write

$$S_e \approx \dot{n} e \varepsilon \tag{15}$$

Combining with Ohm's law (eqn 7) to eliminate the last term on the LHS, and recognizing that $(\nu_{ei}+\nu_{en})\mathbf{j}_e \cdot \mathbf{j}_e >> \nu_{ei} (\mathbf{j}_i \cdot \mathbf{j}_i + \mathbf{j}_e \cdot \mathbf{j}_i)$, we may re-write equation (12) as follows:

$$\frac{\partial}{\partial t}\left(\frac{3}{2} n e T_e\right) - \nabla \cdot \left(\frac{5}{2} T_e \mathbf{j}_e + \kappa_e \nabla T_e\right) \approx \mathbf{E} \cdot \mathbf{j}_e - 3nk \frac{m_e}{m} (\nu_{ei} + \nu_{en})(T_e - T) - \dot{n} e \varepsilon \tag{16}$$

In the equation above we have assumed that the heavy species are in thermal equilibrium at all times with a temperature, $T=T_n=T_i$. The terms in the divergence (LHS) simply denote the flow of heat convected by the electron velocity field, and the heat conducted through the electron fluid, respectively. The first term on the RHS is the rate of work done by the electric field on the electron fluid, and the second term expresses the heat released (generated) in the electron fluid due to collisions with the cooler heavy species.

For the ions and neutrals, we neglect inelastic losses associated with the ionization process and sum the two energy equations to obtain:

$$\frac{\partial}{\partial t}\left(\frac{3}{2} n_n k T\right) + \nabla \cdot \left[\frac{5}{2} nkT \mathbf{u}_i + \mathbf{q}_n\right] - \mathbf{u}_i \cdot \nabla nkT \approx Q_i + Q_n \tag{17}$$

In deriving equation (17) we assumed that $n+n_n \approx n_n$, $\mathbf{u}_n \approx 0$, and $\mathbf{q}_n >> \mathbf{q}_i$ since $\kappa_n/\kappa_i \sim (n_n/n)(\nu_{in}/\nu_{ni}) \sim (n_n/n)^2 >> 1$. The collisional heating terms become,

$$\begin{aligned} Q_i + Q_n = Q_{in} + Q_{ni} + Q_{ne} + Q_{ie} &\approx -\mathbf{R}_{in} \cdot (\mathbf{u}_i - \mathbf{u}_n) + (\nu_{ei} + \nu_{en}) n \frac{2m_e}{m} \frac{3}{2} k(T_e - T) \\ &\approx nm\nu_{in} u_i^2 + (\nu_{ei} + \nu_{en}) n \frac{2m_e}{m} \frac{3}{2} k(T_e - T) \end{aligned} \tag{18}$$

C. Boundary Conditions

The convention followed for the specification of the boundary conditions follows from the finite volume approach (see next section) in which scalar quantities are cell-centered and fluxes are edge-centered. Thus, flux

boundary conditions are set by specifying the flux vector at the boundary while Dirichlet conditions are set by specifying the centered quantity in the imaginary cell ("ghost" cell) that lies outside the computational region. Electron and ion particle fluxes at walls are expressed by the net electron current density and the ion particle flux as follows:

$$\begin{aligned} \mathbf{j}_e \cdot \hat{\mathbf{n}} &= \left(\mathbf{j}_e^{em} + \mathbf{j}_e^{ab}\right) \cdot \hat{\mathbf{n}} \\ \mathbf{j}_i \cdot \hat{\mathbf{n}} &= \mathrm{enu}_B \end{aligned} \tag{19}$$

And the convective heat is expressed by,

$$\left(\mathbf{j}_e T_e\right) \cdot \hat{\mathbf{n}} = \mathbf{j}_e^{em} \cdot \hat{\mathbf{n}} \phi + \mathbf{j}_e^{ab} \cdot \hat{\mathbf{n}} \left(2T_e + \phi\right) \tag{20}$$

The sheath at all walls is assumed to act as a perfect thermal insulator and therefore,

$$\mathbf{q}_e \cdot \hat{\mathbf{n}} = 0 \tag{21}$$

1. Insert Wall (r=R, 0<z<L_{ins})

The emitted electron current density from the insert wall ($\hat{\mathbf{n}} = \hat{\mathbf{r}}$) is given by the Richardson-Dushman equation for thermionic emission,[19]

$$\mathbf{j}_e^{em} \cdot \hat{\mathbf{n}} = \alpha T_w^{\,2} e^{-[e(\phi_{WF} - \phi_{SH})/kT_w]} \equiv \alpha T_{eff}^{\,2} e^{-(e\phi_{eff}/kT_{eff})} \tag{22}$$

Where the effective insert temperature and effective potential are specified by,

$$T_{eff} \equiv T_w^0 - \Delta T\left(z/L_{ins}\right)^{\zeta}, \qquad \phi_{eff} \equiv 1.41 + 5 \cdot 10^{-4} T_{eff} \tag{23}$$

(where ϕ_{eff} is in volts and T_{eff} in °K). The insert temperature profile of the cathode under study has not yet been measured. Thus in the present model we include the field-enhanced emission due to the Schottky effect in an "effective temperature" profile. The constants in equation (23) are specified to match the measured profile[20] (Fig 2) of the insert temperature in a 6.4-mm (outer channel) diameter cathode operated at a discharge current of 12 A (ΔT=200 °K and ζ=0.65). Once the temperature measurements of the cathode under study are available we plan to implement directly the true insert temperature, and properly incorporate the Schottly effect. In the simulations presented in this paper the peak insert temperature is varied until the value of the total current through the orifice matches the operating current of the case under investigation (specifically 25 A of discharge current). Due to the field-enhanced emission we expect the true insert temperature to be lower than presently predicted by the model.

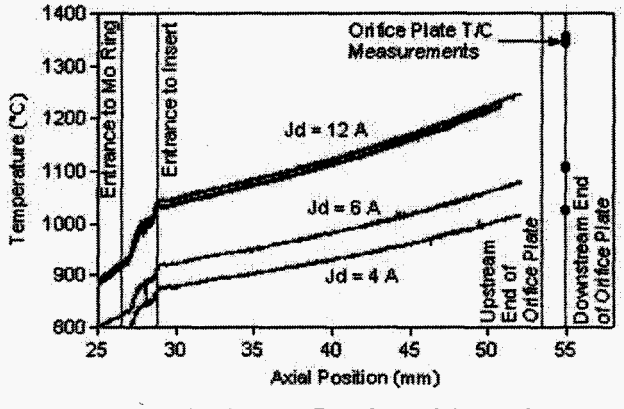

Fig 2. Insert temperature measurements obtained at JPL for a 6.4-mm diameter hollow cathode. (Note that in the above arrangement the orifice plate is to the left and electrons flow out of the orifice from left to right).

The electron current density that escapes the system into the insert wall is given by,

$$\mathbf{j}_e^{ab} \cdot \hat{\mathbf{n}} = -\frac{en\bar{c}_e}{4} e^{-(e\phi/kT_e)} \tag{24}$$

while ions are assumed to leave the system into the walls at the Bohm velocity:

$$\mathbf{j}_i \cdot \hat{\mathbf{n}} = en\sqrt{kT_e/m} \tag{25}$$

Finally, we assume that the temperature of the heavy species at the walls equals the wall temperature. Thus,

$$T = T_{eff} \tag{26}$$

2. Orifice plate & conductor walls ($z=0$, $r_{orf}<r<R$ & $r=R$, $z>L_{ins}$)
The emission characteristics of the remaining walls are unknown so we assume the limiting case of zero electron emission,

$$\mathbf{j}_e^{em} \cdot \hat{\mathbf{n}} = 0 \tag{27}$$

However, both electrons and ions are permitted to escape at a rate given by equations (24) and (25) respectively. The convective heat flux is given by equation, with the temperature at the conducting wall (following the insert) set to,

$$T_w = T_w^0 - \Delta T \tag{28}$$

At the orifice plate the wall temperature is given by:

$$T_w = T_w^0 \tag{29}$$

The heavy species temperature is set equal to the wall temperature,

$$T = T_w \tag{30}$$

3. Orifice ($z=0$, $0<r< r_{orf}$)
At the orifice, we implement Dirichlet boundary conditions for the plasma density and potential:

$$n_{orf} = 1.5 \cdot 10^{20}\ m^{-3}, \phi_{orf} = 12.5\ V \tag{31}$$

which are based on measurements. An adiabatic condition is set for the electron temperature.

4. Gas Inlet ($z=L$, $0<r<R$)
At the cathode channel inlet no net electron flux is permitted in or out of the computational region:

$$\mathbf{j}_e \cdot \hat{\mathbf{n}} = 0 \tag{32}$$

but ions are allowed to escape at the ion thermal speed:

$$\mathbf{j}_i \cdot \hat{\mathbf{n}} = en\sqrt{kT/m} \tag{33}$$

The temperature of the heavy species is held fixed and equal to the conducting wall temperature:

$$T = T_w^0 - \Delta T \tag{34}$$

As in the orifice, an adiabatic condition is placed on the electron temperature. Symmetry boundary conditions are implemented along the axis of symmetry.

III. Numerical Approach

1. Finite differencing of conservation equations

The conservation equations are discretized using a finite volume approach. The principal advantage of this approach is that conservation laws involving the vector integral theorems are usually well respected by the differencing since the differencing is derived from those theorems. More specifically, the divergence theorem states that if V is the volume bounded by a closed surface S, and Γ is a vector function with continuous derivatives, then

$$\iiint_V \nabla \cdot \boldsymbol{\Gamma} dV = \iint_A \boldsymbol{\Gamma} \cdot \hat{\mathbf{n}} dA \tag{35}$$

If ΔV is a discrete volume in 3-D space described by a single cell in the computational grid bounded by area ΔA, and if $\nabla \cdot \boldsymbol{\Gamma}$ and $\boldsymbol{\Gamma} \cdot \hat{\mathbf{n}}$ are uniform over the cell volume and its faces then we can write:

$$(\nabla \cdot \boldsymbol{\Gamma})_{\text{cell}} \Delta V = \sum_{\ell=\text{cell face}}^{\text{all cell faces}} (\boldsymbol{\Gamma} \cdot \hat{\mathbf{n}})_\ell \Delta A_\ell \tag{36}$$

which defines a finite volume difference form for the divergence operator. In the numerical model presented here all fluxes are edge-centered while scalars are cell-centered quantities. The fluxes are determined using second-order accurate finite differences. The computational grid used to solve the equations is a uniform grid with 0.5 mm x 0.5 mm cells.

2. Evolution of conservation equations to steady state

The conservation equations for the plasma-gas system are evolved to steady state using time-marching for the plasma density and electron temperature. That is, the time-dependent form of the equations is in fact solved until steady state is attained for all variables. By combining equations (2), (7) and (8) we eliminate the ion velocity to obtain the following:

$$\frac{\partial n}{\partial t} = \nu_{iz} n - \nabla \cdot \left\{ \frac{e^{-1} m_e \nu_{en} \mathbf{j}_e - \nabla[nk(T + T_e)]}{m \nu_{in} (1 + \nu_{iz} / \nu_{en})} \right\} \tag{37}$$

(with T and T_e expressed in eV). Adding the steady state electron and ion continuity equations yields,

$$\nabla \cdot (\mathbf{j}_e + \mathbf{j}_i) = 0 \tag{38}$$

and combining with generalized Ohm's Law we obtain,

$$\nabla \cdot \left(\frac{\nabla \phi}{\eta} \right) = \nabla \cdot \left[\frac{\nabla (n T_e)}{\eta n} + \mathbf{j}_i \left(1 - \frac{\nu_{ei}}{\nu_{en} + \nu_{ei}} \right) \right], \quad \eta = \frac{m_e (\nu_{en} + \nu_{ei})}{ne^2} \tag{39}$$

The approach to solve the complete system of equations is summarized in Fig 3. Initial estimates of the electron current density vector field, plasma density and electron temperature are used to compute all the required fluxes, transport coefficients and related quantities. Equations (37) and (16) are then time-marched to compute new values of n and T_e. The evolution of these equations at fixed current density is repeated for N iterations. When N reaches a user-specified number, equation (39) is solved implicitly to determine a new value of the electric potential, ϕ, which is in turn used to compute a new electric vector field from $E=-\nabla\phi$. The electron current density vector field is then updated using Generalized Ohm's law (eqn (8)). Concurrently, equation (17) is solved implicitly to determine a new heavy species temperature, T. Assuming uniform neutral gas pressure throughout the channel the neutral particle density is updated using the ideal gas law, $n_n=p_n/kT$, talking into account the partial pressure from electrons and ions,

$$n_n = \frac{p - nk(T_e + T)}{kT} \tag{40}$$

The value of the total gas pressure used in the simulations is based on experimental measurements taken at the gas inlet.[12] The procedure is repeated until the solution for all quantities has reached steady state.

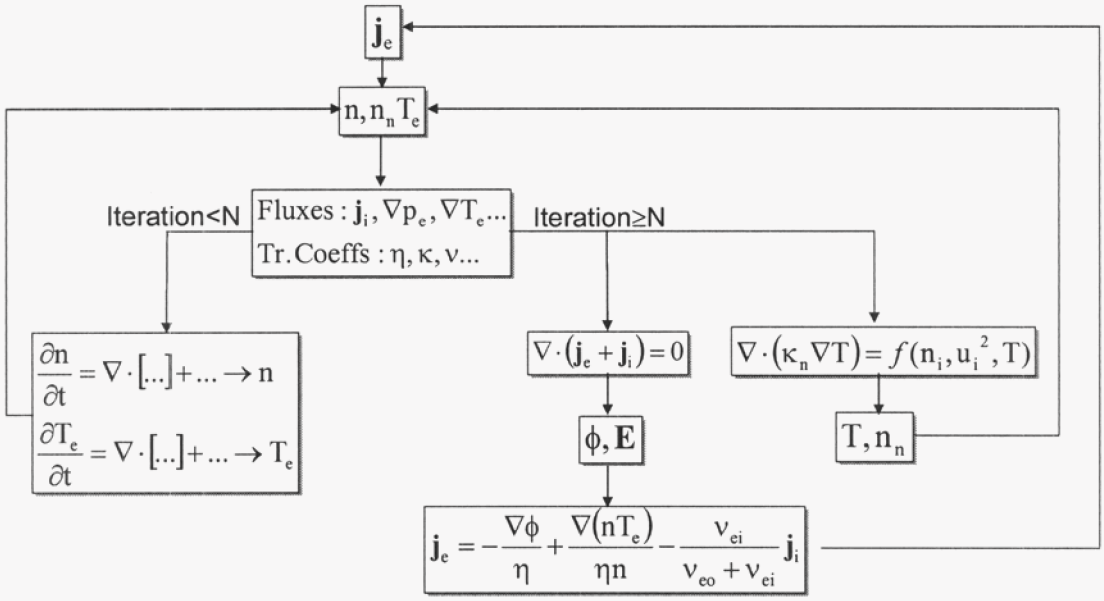

Fig 3. Approach for obtaining the steady-state solution of the conservation equations.

IV. Model Results and Comparisons with Measurements

Figure 6 shows the computed plasma density overlaid by electron current density streamlines. Immediately apparent is a non-monotonic behavior exhibited by the plasma density along the hollow cathode channel, which is contrary to previous experimental observations in lower current, smaller size cathodes.[4,7] The theoretical results are supported by experimental observations recently obtained at JPL in the cathode simulated by the theoretical model. It is suggested that the non-monotonic behavior is mainly due to the larger channel size associated with the high-current cathode. The larger open area of the orifice allows sufficiently high rates of plasma flow out of the cathode so that the rate at which electrons are supplied by the emitter surface is insufficient to replenish the plasma lost through the orifice. Moreover, since plasma is also lost into the orifice plate through the sheath, the larger orifice plate area also enhances the rate of plasma loss from the cathode.

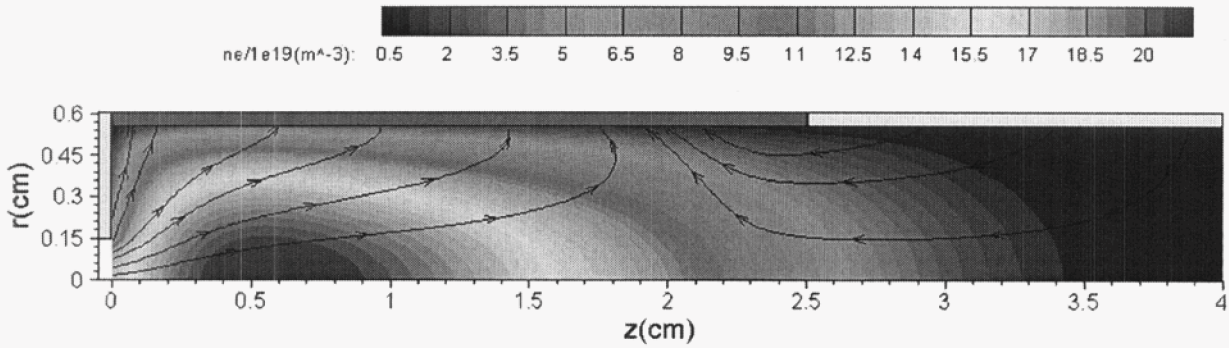

Fig 4. Computed plasma particle density and electron current density streamlines in the hollow cathode insert region.

A comparison between the computed plasma density at the centerline as a function of distance from the orifice entrance is shown in Fig 5. The measurement in Fig 5 was obtained at a discharge current of 25 A and a gas flow

rate of 5.5 sccm. The data for the 5.5 sccm case was obtained after the cathode had been operated for an additional ~250 hours compared to the 5 and 4.3 sccm cases, which have been normalized (to emphasize differences in the displacement of the density profile) and are compared with the 5.5 sccm data (also normalized) in Fig 6. The theoretical curve in Fig 5 corresponds to the 5 sccm case for which a measurement of the gas pressure during operation of the cathode (1.07 Torr) exists. Although the theoretical result is within the experimental error, a few qualitative disagreements must be noted.

First, it is seen that the model predicts the location of the of peak plasma density to be approximately 0.25 cm farther upstream of the orifice entrance. However, the measurements for both the 4.3 and 5 sccm cases (Fig 6) show the peak to be at the location predicted by the model. To be more quantitative, by comparison with the 5 sccm case the 5.5 sccm measurements (at +250 hrs) suggest that about a factor of 1.1 (10%) increase in the gas flow rate is followed by about a factor of 3 in the displacement of the location of the peak density (0.6 cm at 5 sccm to 0.2 cm at 5.5 sccm). Additional comparisons between the 5.5 sccm case and a 10 sccm case, operated at the same discharge current and,[12] confirm that the location of the peak moves toward the orifice entrance with increasing flow rate. However, the 5.5 and 10 sccm comparison also shows that the displacement factor is about 4 for a 1.8 increase in the flow rate (0.2 cm at 5.5 sccm to 0.05 at 10 sccm). Although the relationship between flow rate and peak density location may certainly be non-linear it is believed that conditioning of the insert after a few hundred hours of operation is partially responsible for the displacement. It is noted that the data for the 10 sccm case was also obtained after the cathode had been operated for an additional ~250 hours compared to the 5 and 4.3 sccm cases. Also noted is the slope change downstream (i.e. to the left) of the peak density location which further supports the possibility of changing emission characteristics with time of operation rather than experimental errors associated with the alignment of the probe. In the absence of insert temperature measurements for the cathode modeled in this effort (it is recalled that we implement in the model the temperature profile of a smaller cathode, operating at 12 A) it is not possible to delineate quantitatively the magnitude of the conditioning effects.

Second, the model predicts less steep density gradients upstream and downstream of the density maximum. Downstream (left) of the peak, the disagreement may be associated with the conditioning effects alluded to in the previous paragraph. It should be noted that the agreement between theory and experiment at the orifice entrance (z=0) is of no significance since the boundary condition in the model is set to match the experimental value. Contrary to the comparisons with the 5.5 sccm (+250 hrs) case, numerical simulations using the density boundary condition from the 5 and 4.3 sccm cases reveal excellent agreement with that set of data. Thus, all the aforementioned comparisons with plasma density emphasize the need for temperature data of the insert, which we plan to obtain at JPL in the near future.

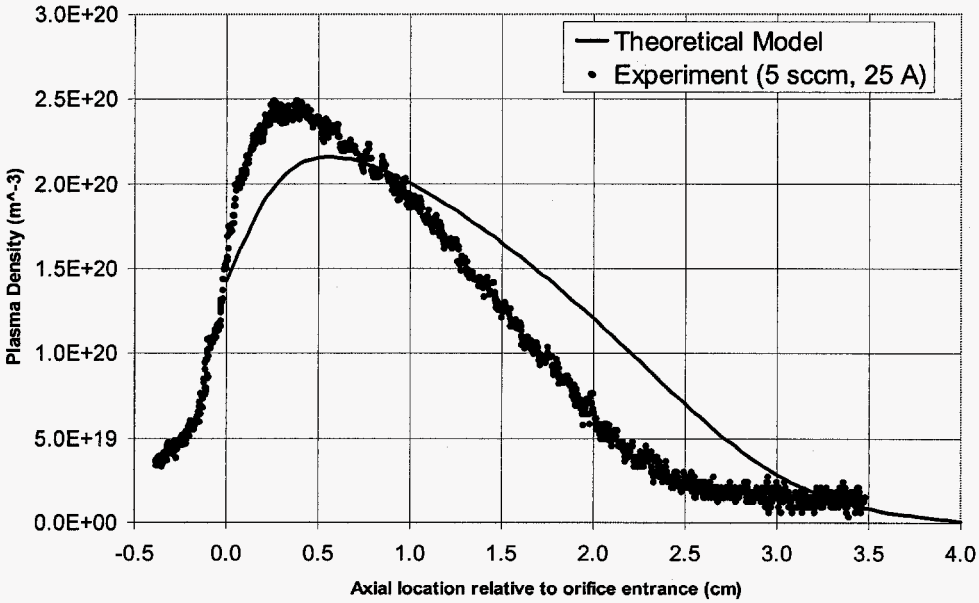

Fig 5. Comparison between model results and measurements taken for 5 sccm, at a discharge current of 25 A.

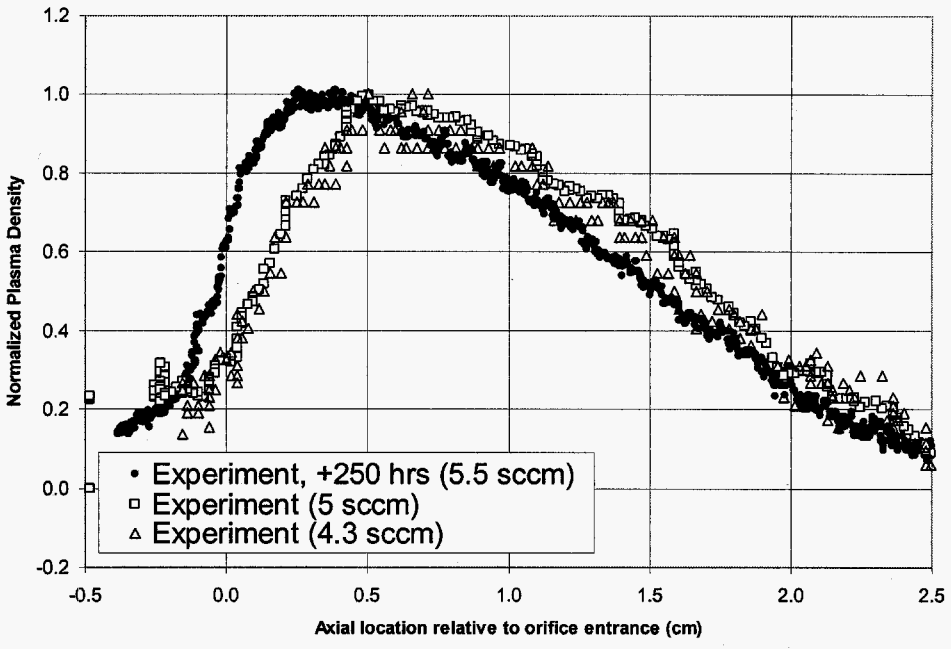

Fig 6. Comparison between two plasma density measurements at 5.5, 5 and 4.3 sccm (at discharge current of 25 A). The 5.5 sccm measurements were obtained after the cathode had been operated for an additional ~250 hrs.

Additional comparisons are depicted in Fig 7 for the plasma potential and electron temperature. The corresponding 2-D model results are shown in Fig 10 and Fig 11, respectively The agreement between both plasma potential and electron temperature is excellent upstream of $z \approx 2.2$ cm. However, it must be noted that the agreement between theory and experiment for the plasma potential at z=3 cm is of no significance since the potential boundary condition in the model is set to match the last available experimental value (which is at z=3 cm). The reason for this choice is that our calculations and comparisons with the experiment suggest that far upstream of the orifice (z>~2cm) mass and heat transport occur classically. This is supported by the excellent agreement between the model (which assumes classical transport throughout the insert region) and the measurements, for both plasma potential and electron temperature, for z>~2 cm. Closer to the orifice however, the measurements indicate a rise in the potential and electron temperature compared to the model predictions. The computational result is in agreement with Generalized Ohm's law (eqn (7)). In the absence of the Hall effect, which is assumed in our model based on the relatively low Hall parameter in this region (see Table 1), the electric field is driven by two competing processes: plasma resistance and electron pressure gradients ($-\mathbf{E}=\nabla\phi \approx -\eta \mathbf{j}_e + \nabla p_e/en$). The comparison suggests that classical resistivity (eqn (39), right) is insufficient to account for the heating that is observed by the measurements. Specifically, the model predicts T_e=1.83 eV at z=0 compared to the measured value of 3.4 eV. Anomalous heating in this region may occur as a result of two-stream instabilities. Buneman[21] (1959) showed that if the relative (e-i) drift velocity exceeds $\sim(kT_e/m_e)^{1/2}$ it is possible to excite waves associated with the electron motion (and thus are of high frequency) with rapid growth rates, that can lead to anomalously enhanced resistivity and plasma heating. If the relative drift velocity is sufficiently higher that the electron thermal speed, these waves can be excited regardless of whether the ions are in thermal equilibrium with the electrons. Later (1964), Stringer[22] showed that if the ratio of the ion-to-electron temperature is low it is possible to excite additional instabilities at relative velocities much lower than the electron thermal speed. Figure 8 depicts Stringer's calculations for a hydrogen plasma (m_i/m_e=1836). As a comparison, the values computed by the hollow cathode model for $M=u_{drift}/(kT_e/m_e)^{1/2}$ and T_i/T_e are shown in Fig 9. The model values suggest that it is possible for the insert plasma to be subject to a variety of counterstreaming instabilities, other than the Buneman (e-e) instability; however to quantify them it would be necessary to perform growth rate analysis for the heavier xenon ions (m_i/m_e=241067).

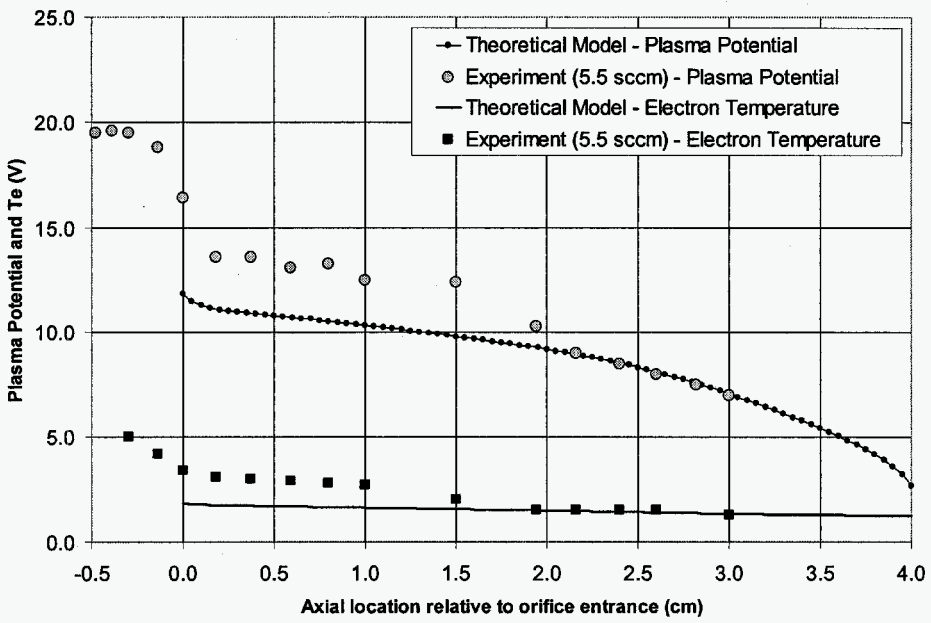

Fig 7. Comparison between model results and measurements for the plasma potential and electron temperature.

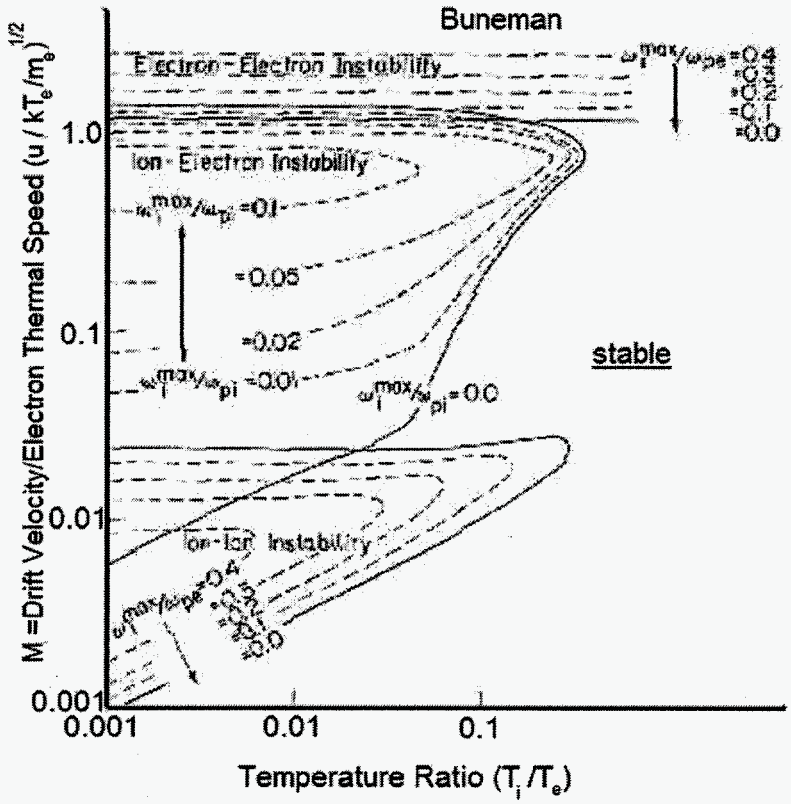

Fig 8. Growth rate of the fastest-growing wavelength in a countersteaming plasma (m_i/m_e=1836) as a function of the drift velocity/$(kT_e/m_e)^{½}$ and the ion-to-electron temperature ratio. (After Ref. 22)

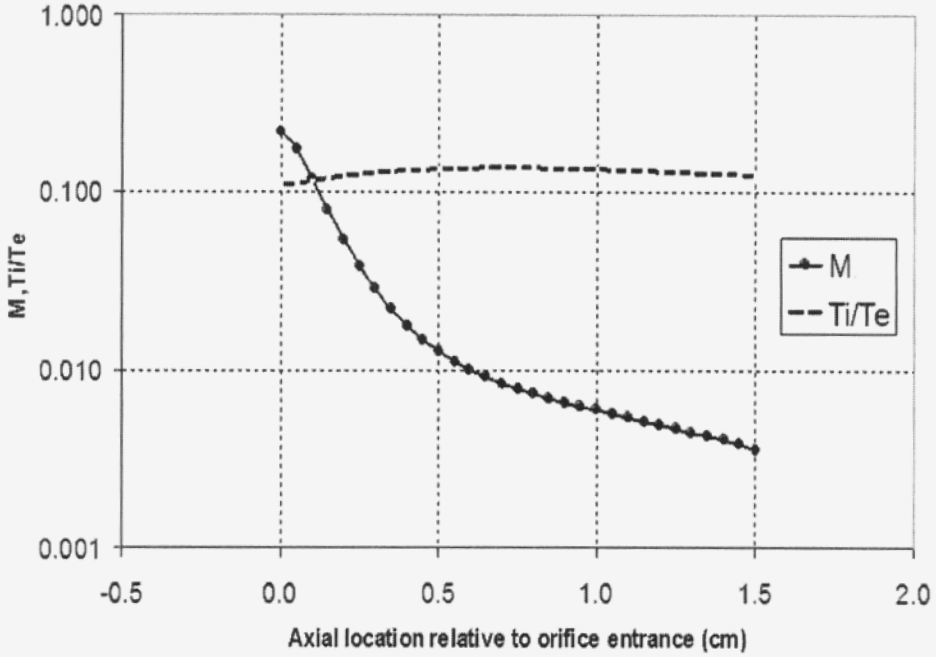

Fig 9. Ratio of relative drift velocity over $(kT_e/m_e)^{1/2}$ (Mach number) computed along the axis of symmetry.

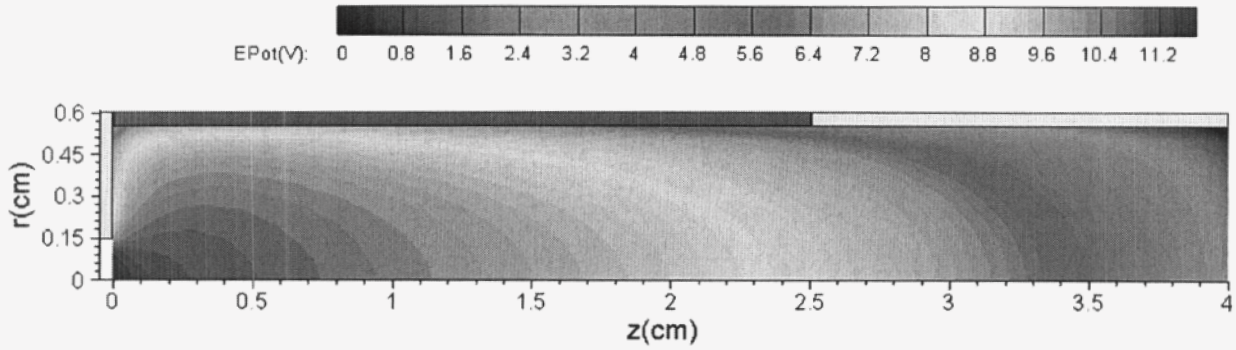

Fig 10. Computed plasma potential in the hollow cathode insert region.

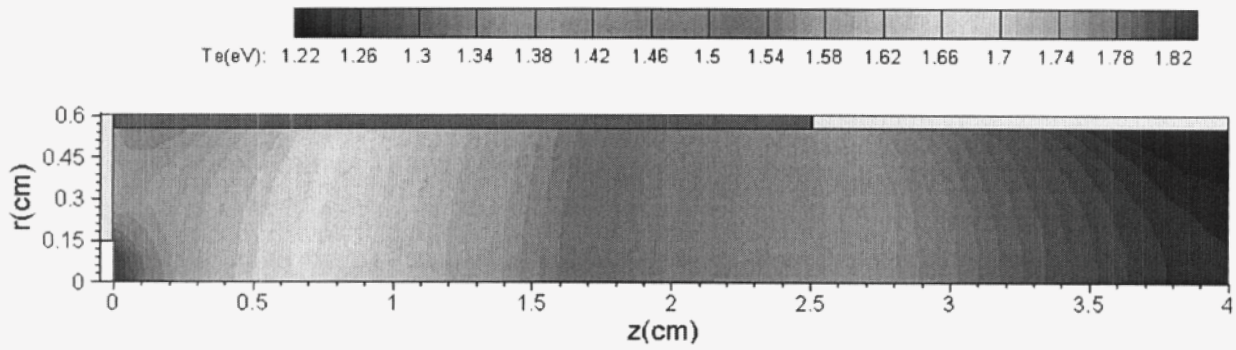

Fig 11. Computed electron temperature in the hollow cathode insert region.

The solution to the heavy species energy equations, along with the assumption of uniform gas pressure along the channel allows us to compute self-consistently with the plasma conservation equations, the heavy species temperature and particle density of the neutrals. The solution is illustrated in Fig 12 (temperature) and Fig 13 (particle density). Similar heavy species temperatures have been predicted by other authors.[23,12]

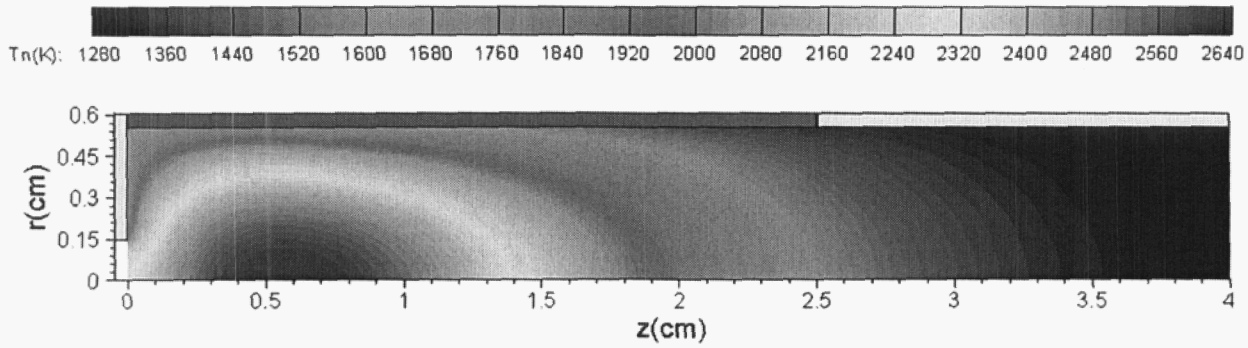

Fig 12. Computed heavy-species temperature in the hollow cathode insert region.

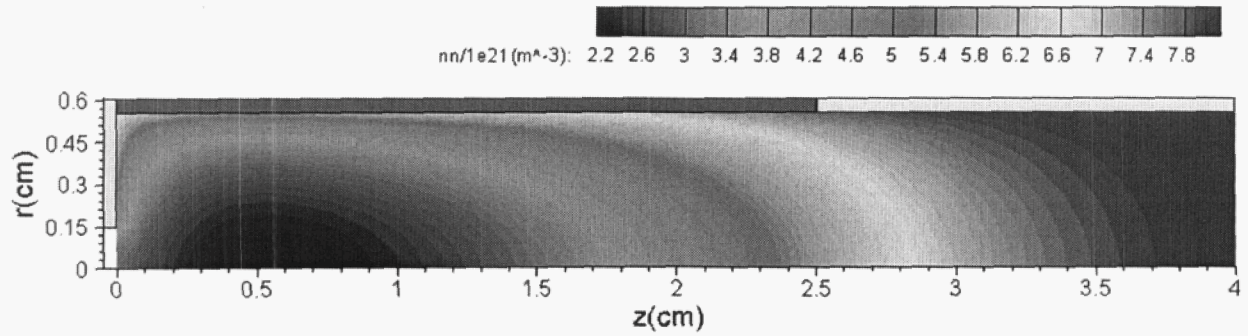

Fig 13. Computed neutral particle density in the hollow cathode insert region.

Table 2 lists the distribution of power in the insert region as well currents to surfaces. Approximately 90% of the electric power ($\mathbf{E}\cdot\mathbf{j}_e$) associated with the electrons is used to (partially) ionize the neutral gas. A small percentage (2%) is used to heat the heavy species while the remaining power (9%) escapes as heat from the insert region. Almost 35 A of electron current is found to be emitted by the insert while 30% of that (10.1 A), which includes both emitted electrons and ionization electrons, return to the emitter surface. Approximately 3.5 A of ions also impact the emitter surface.

Table 2. Power and current balance in the hollow cathode insert region.

Power Balance (W)			Current Balance $I_s = \iint_A \mathbf{j}_s \cdot (\hat{\mathbf{n}} dA)$	
			Emitted (A)	Absorbed (A)
Conv.+Condv. Heating	-5.1	Orifice Plate	$I_e = 0.0$ $I_i = 0.0$	$I_e = -1.35$ $I_i = 0.52$
Electric Power ($\mathbf{E}\cdot\mathbf{j}_e$)	56.2	Insert Wall (Emitter)	$I_e = 34.7$ $I_i = 0.0$	$I_e = -10.1$ $I_i = 3.47$
Ionization (loss)	-49.8	Conductive Wall	$I_e = 0.0$ $I_i = 0.0$	$I_e = -1.86$ $I_i = 0.14$
Thermal Equilibration (loss)	-1.3	Orifice	$I_e = -24.98$ $I_i = -0.02$	

V. Conclusion

The 2-D axisymmetric model presented in this paper has largely been motivated by the need to quantify plasma properties at the emitter surface, in order to assess the effects of the plasma on insert lifetime. Previous simplified models, and experimental measurements at the axis of symmetry alone are not sufficient to provide the level of detail required at the emitter for the assessment life expectancy. The need to rigorously determine fluxes to the emitter surface has steered the present model beyond the phenomenological models (0-D or 1-D) that have been formulated thus far. In particular, the classical processes believed to drive the evolution of the plasma properties in the insert region have been included through a set of multiple species, fluid-like conservation equations, which are solved numerically in a self-consistent manner, in 2-D geometry. All relevant collision cross sections have been taken from previously published work. Electron emission characteristics have been modeled after the Richardson equation for thermionic emission and are based on existing measurements of the insert temperature from a smaller size cathode. Thus, the model must be upgraded with the measurements from the simulated cathode/insert before the numerical results can be unambiguously compared to the existing plasma measurements.

Nevertheless, in the expectation that the insert temperature profile will not be drastically different than the one used in the model, a number of conclusions may be drawn from the results and comparisons with the recent data obtained at JPL. The model suggests that the dominant heating mechanism of the neutral gas is resonant charge-exchange collisions between fast ions and slow neutrals. It is possible that additional heating may be due to viscous effects that have been neglected in the present effort. Also possible is additional ion heating from anomalous effects that have also been neglected in the present effort. Specifically, model predictions for the relative drift velocity and ion-to-electron temperature ratio suggest that the insert plasma may be in a regime where two-stream instabilities are anomalously heating the plasma. The comparisons with the data support this conclusion. The data show approximately a factor of two higher electron temperature at the orifice entrance. To account for this heating the classical plasma transport models must be re-formulated to include anomalous effects.

Appendix

The mean thermal speeds for a species "s" is given by,

$$\bar{c}_s = \sqrt{8kT_s / \pi m_s} \tag{41}$$

where T_i=T and m_i=m. The e-n "collision frequency" ν_{en} uses a numerical fit to the collision cross section based on data from Ref. 15, averaged over a Maxwellian distribution.

$$\nu_{en} = n_n \bar{c}_e \frac{\sqrt{\pi}}{2\sqrt{2}} \frac{6.6 \cdot 10^{-19}(0.25T_e - 0.1)}{1 + (0.25T_e)^{1.6}} \tag{42}$$

The i-n "collision frequency" is dependent upon the ion drift velocity. The dependence of the average number of collisions per unit time, per particle "i" at speed $\bar{u}_i$, with particles of kind "n" – the "collision frequency" – is found in Ref. 24. For the present problem, we can express the drift-dependent, i-n frequency as follows:

$$\nu_{in} = n_n \langle \sigma u \rangle_{in} = n_n \sigma_{CEX} \sqrt{\frac{2kT}{\pi m}} \left[e^{-x^2} + \left(2x + \frac{1}{x} \right) \frac{\sqrt{\pi}}{2} \mathrm{erf}(x) \right]$$
$$x \equiv \bar{u}_i / \sqrt{\frac{2kT}{m}}, \quad \sigma_{CEX} = 10^{-18} m^2 \tag{43}$$

The value for σCEX is taken from Ref. 25. The e-i (coulomb) collision frequency is given by,[26]

$$\nu_{ei} = 2.9 \cdot 10^{-12} n T_e^{-3/2} \left[23 - 0.5 \ln \left(\frac{10^{-6} n}{T_e^3} \right) \right], \quad T_e < 10 eV \tag{44}$$

The ionization collision frequency incorporates numerical fit to measurements obtained by M. Hayashi,[27] where ε =12.127 eV.

$$\nu_{iz} = n_n \bar{c}_e \sigma_{iz} = n_n \bar{c}_e \cdot 10^{-20}\left(3.97 + 0.643 T_e\right) e^{-\varepsilon/T_e} \tag{45}$$

Using the form derived in Ref. 14 for the electron thermal conductivity in the limit of B=0 we write,

$$\kappa_e = 3.16 \frac{e^2}{m_e} \frac{n T_e}{\left(\nu_{ei} + \nu_{en}\right)} \left(\frac{W}{meV}\right) \tag{46}$$

to take into account e-n collisions. The thermal conductivity for the neutral gas is given by,[28]

$$\kappa_n = 0.083 \frac{\sqrt{T/M}}{\delta^2 \Omega(\bar{T})} \left(\frac{W}{m°K}\right) \tag{47}$$

where,

$$\Omega = 0.015 \bar{T}^{0.05} + 0.113 e^{-\bar{T}} + 1.141 \bar{T}^{-0.15}, \qquad 1 < \bar{T} < 50 \tag{48}$$

$$\bar{T} \equiv T/229, \ \delta = 4.055 Å, \ M = 131.3 amu \tag{49}$$

Acknowledgments

The research described in this paper was carried out by the Jet Propulsion Laboratory, California Institute of Technology, under a contract with the National Aeronautics and Space Administration.

References

[1] Sarver-Verhey, T.R., "Destructive Evaluation of a Xenon Hollow Cathode After 28,000 Hour Life Test," AIAA Paper 98-3482, July 1998.
[2] Sengupta, A., Brophy, J. R., Goodfellow, K. D." Status Of The Extended Life Test Of The Deep Space 1 Flight Spare Ion Engine After 30,352 Hours Of Operation", AIAA Paper 03-4558, July 2003.
[3] Palluel, P., and Shroff, A.M., "Experimental Study of Impregnated-Cathode Behavior, Emission, and Life," *Journal of Applied Physics*, Vol. 51, No. 5, 1980, pp. 2894-2902.
[4] Siegfried, D.E., and Wilbur, P.J., "An Investigation of Mercury Hollow Cathode Phenomena," AIAA Paper 78-705, April 1978.
[5] Salhi, A., "Theoretical and Experimental Studies of Orificed, Hollow Cathode Operation," Ph.D. Dissertation, Aeronautics and Astronautics Dept., Ohio State Univ., Columbus, OH, 1993.
[6] Rawlin, V.K., "A 13,000 Hour Test of a Mecury Hollow Cathode," NASA TM X-2785, 1973.
[7] Domonkos, M.T., Gallimore, A.D., Williams, G.J., Patterson, M.J., AIAA Paper 99-2572, June 1999.
[8] Mirtich, M.J., "Investigation of Hollow Cathode Performance for 30-cm Thrusters," NASA TM X-68298, 1973.
[9] Friedly, V. J., and Wilbur, P. J., "High Current Hollow Cathode Phenomena," *Journal of Propulsion and Power*, Vol. 8, No. 3, 1992, pp. 635-643.
[10] Siegfried, D.E., and Wilbur, P.J., "A Model for Mercury Orificed Hollow Cathode: Theory and Experiment," AIAA Paper 82-1889, Nov. 1982.
[11] Salhi, A., and Turchi, P.J., "A First Principles Model for Orificed Hollow Cathode Operation," AIAA Paper 92-3742, July 1992.
[12] Goebel, D.M., Sengupta, A., Watkins, A. and Jameson, K. "Hollow Cathode and Keeper-Region Plasma Measurements Using an Ultra-Fast Miniature Scanning Probe," AIAA Paper 04-3430, July 2004.
[13] Katz, I., Anderson, J.R., Polk, J.E., and Brophy, J.R., "One-Dimensional Hollow Cathode Model," *Journal of Propulsion and Power*, Vol. 19, No. 4, 2003, pp. 595-600.
[14] Braginskii, S.I., "Transport Processes in Plasmas," *Reviews of Plasma Physics*, Vol. 1, pp. 205-311, 1965.

[15] Hayashi, M., "Determination of Electron-Xenon Total Excitation Cross-Sections from Threshold to 100eV, from Experimental Values of Townsend's α," *J. Phys. D: Appl. Phys.*, Vol 16, 1983, pp. 581-589.
[16] Spitzer, L., *Physics of Fully Ionized Gases*, Interscience Publishers, Inc., New York, 1956, pp. 86-88.
[17] Griem, H.R., *Plasma Spectroscopy*, Academic Press, New York, 1966.
[18] Malik, A.K., Montarde, P., and Haines, M.G., "Spectroscopic Measurements of Xenon Plasma in a Hollow Cathode," *Journal of Physics D: Applied Physics*, Vol. 33, No. 16, 2000, pp. 2037-2048.
[19] Dushman, S., "Electron Emission from Metals as a Function of Temperature," *Phys. Rev.*, Vol. 21, No. 6, 1923, pp. 623-636.
[20] Polk, J., *et al.*, "Temperature Distributions in Hollow Cathode Emitters," AIAA Paper 04-4116, July 2004.
[21] Buneman, O., "Dissipation of Currents in Ionized Media," *Phys. Rev.*, Vol. 115, No. 3, 1959, pp. 503-517.
[22] Stringer, T.E., "Electrostatic Instabilities in Current-Carrying and Counterstreaming Plasmas," *Plasma Physics, J. Nucl. Energy, Part C*, Vol 6, 1964, pp. 267-269.
[23] Williams, G., Smith, T., Domonkos, M., Shand, K., and Gallimore, A., "Laser Induced Fluorescence Characterization of Ions Emitted from a Hollow cathode," AIAA Paper 99-2862, Los Angeles, CA, June 1999.
[24] Chapman, S., and Cowling, T.G., *Mathematical Theory of Nonuniform Gases*, Cambridge University Press, Cambridge, England, 1953, pp. 90-92.
[25] Miller, J.S., Pullins, S.H., Levandier, D.J., Chiu, Y., and Dressler, R.A., "Xenon Charge Exchange Cross Sections for Electrostatic Thruster Models," *Journal of Applied Physics*, Vol. 91, No. 3, 2002, pp. 984-991.
[26]Book, D.L., *NRL Plasma Formulary*, Naval Research Laboratory, Washington D.C., 1987, pp. 33-34, 38.
[27] Hayashi, M., "Determination of Electron-Xenon Total Excitation Cross-Sections from Threshold to 100eV, from Experimental Values of Townsend's α," *J. Phys. D: Appl. Phys.*, Vol 16, 1983, pp. 581-589.
[28] Hirschfelder, J.O., Curtiss, C.F., and Bird, R.B., *Molecular Theory of Gases and Liquids*, John-Wiley, New York, 1964, pp. 534, 1110, 1126-1127.